Efficient nitrate removal from water using an integrated photocatalyst-adsorbent based on chitosan-titanium dioxide nanocomposite

Smitha Venu Sreekala (smithavs2007@gmail.com)
Centre for Water Resources Development and Management https://orcid.org/0000-0002-4829-0372
Athulya Parola
Centre for Water Resources Development and Management
Vimala Thaimani
Centre for Water Resources Development and Management
Harikumar Puthenveedu Sadasivan Pillai
Centre for Water Resources Development and Management
Resmi Thoppil Ramakrishnan
Centre for Water Resources Development and Management

Research Article

Keywords: sol-gel, chitosan, titanium dioxide, nanocomposite, photocatalysis, nitrate reduction, adsorption

Posted Date: September 15th, 2022

DOI: https://doi.org/10.21203/rs.3.rs-1980945/v1

Version of Record: A version of this preprint was published at Environmental Science and Pollution Research on December 28th, 2022. See the published version at https://doi.org/10.1007/s11356-022-24895-5.

Abstract

An increased discharge of nitrates to the natural water resources was observed across the globe due to various anthropogenic activities resulting in environmental pollution and associated harmful effects. In the present work, sol-gel-derived functional nanocomposites based on silver (Ag) doped titanium dioxide (TiO_2) coated chitosan nanocomposites were successfully synthesized in the form of beads and their application for the removal of nitrates from the water was studied. The synthesized nanocomposite beads were further characterized for their structural, textural, and morphological features using X-ray Diffraction Analysis, Fourier Transform Infrared Spectroscopy, UV-Visible Spectroscopy, BET Surface Area analysis, Scanning Electron Microscopy, and Transmission Electron Microscopy. A uniform coating of doped titania species on the chitosan porous structure was achieved through electrostatic interaction. Adsorption/ photocatalytic reduction of nitrates was further monitored by measuring the concentration of nitrate ions in the model contaminated water in the presence of functional nanocomposite beads when subjected to an adsorption study under dark conditions and photocatalytic study under UV/sunlight for a definite time. Drying conditions of the nanocomposite beads were found to have a significant effect on the adsorption cum photocatalysis efficiencies of the nanocomposite. The freeze-dried chitosan-titania nanocomposite beads containing 0.5 mol% Ag exhibited an adsorption efficiency of ~ 43.5% (under dark for 30 min) and photocatalytic reduction capability of ~ 95% (under sunlight for 2 hours), whereas the adsorption and photocatalytic efficiencies were 40% (under dark for 30 min) and 70% (under UV light for 2 hours) respectively, in the case of oven-dried nanocomposite beads, towards the removal of nitrate ions in an aqueous solution. Continuous flow adsorption cum photocatalytic study using the oven-dried nanocomposite beads was carried out further with the help of an experimental setup fabricated in-house and under varying experimental conditions such as flow rate, bed height, and concentration of feed solution. A nitrate removal efficiency of 87.6% and an adsorption capacity of 7.9 mgg^{-1} were obtained for the nanocomposite beads in the continuous flow adsorption cum photocatalysis experiment for up to 8 hours when using an inlet concentration of 100 ppm, bed height 12 cm and flow rate 5.0 $mlmin^{-1}$. A representative fixed-bed column adsorption experiment using a real groundwater sample collected from the Palakkad District of Kerala was also performed using the oven-dried functional nanocomposite beads that show promising results for nitrate removal (85.9% efficiency) along with a significant removal rate for the other anions as well. Thus, the adsorption cum photocatalytic nitrate reduction ability of the synthesized functional material makes them suitable for the efficient removal of nitrates from water/wastewater through an integrated nanocomposite approach.

1. Introduction

Globally, quality aspects of the available natural water resources are getting stressed due to various anthropogenic activities that raise huge concerns for the sustainable development on earth (Mehran et al. 2017). Nitrate contamination of groundwater is identified as a major threat to human health which is contributed by various anthropogenic activities such as intense use of fertilizers, septic and sewage systems, and municipal wastes (Shukla et al. 2019). The permissible limit of nitrates in drinking water is

10 mg/L according to WHO (Ward et al. 2018) and an excess nitrate intake in humans leads to diseases like methemoglobinemia, cancer, etc. Hence, the efficient removal of nitrates from the contaminated water resources before their use for drinking purposes is very important (Huno et al. 2018).

Conventional water treatment methods such as filtration, and lime/soda ash softening could not remove nitrates from drinking water (Dahab et al. 1991). Even though various physicochemical and biological techniques such as reverse osmosis, electrodialysis, chemical precipitation, ion exchange, bio-denitrification, etc. are available for the removal of nitrates from drinking water, the high cost, energy, and post-treatment requirements involved in them limit their practical applications (Archna et al. 2012; Mohsenipour et al. 2014). Photocatalytic reduction of nitrates into harmless nitrogen gas is a relatively new technique for nitrate removal and titanium dioxide is the most widely used material in this regard (Yang et al. 2013; Silva et al. 2018).

Titanium dioxide (TiO_2), a semiconductor material has got wide environmental applications, especially in the field of water treatment for the removal of various pollutants such as organic dyes, heavy metals, harmful anions such as nitrates, phosphates, etc. due to its low toxicity, low cost, high physical/chemical stability and unique photocatalytic activity (Liu et al. 2022). Photocatalytic property of titanium dioxide depends on the crystalline phase and surface area of the material and the wide band gap energy of 3.2 eV usually limits its application under UV light which demands band gap modification to enable its use under sunlight/visible light (Marcelino et al. 2019). Titanium dioxide when doped with silver (Ag) ions modifies its band gap thereby generating electron-hole pairs when excited under sunlight/visible light and the photo-generated electrons can be used for the reduction of nitrates into nitrogen gas (Doudrick et al. 2012). On the other hand, chitosan, a biopolymer is an efficient bio sorbent for nitrate removal (Banu et al. 2021). Chitosan in acidic media is reported to enhance the adsorptive removal of nitrates because of its cationic property and electrostatic interaction. The major shortcomings of chitosan such as its poor chemical stability and mechanical strength (Szymańska et al. 2015) can be solved when it is appropriately incorporated into a nanocomposite system as it may result in tunable properties and synergistic effects. Hence a nanocomposite system of chitosan and titanium dioxide would be an ideal choice for adsorption cum photocatalytic applications for the removal of nitrates from water/wastewater.

A novel 2D Ag-TiO_2/γ-Al_2O_3/chitosan nano-composite photocatalyst was fabricated (Zarei et al. 2020) for enhanced photocatalytic reduction of nitrate through a sol-hydrothermal method and their results show that Ag-doped hybrid heterostructures can effectively utilize UV–visible-light to remove nitrate with an efficiency of 74% in 5 min reaction time. TiO_2-graphene/chitosan nanocomposite system and its application for the removal of anionic dyes was studied (Mohammadi et al. 2020) which demonstrated an excellent photocatalytic enhancement over TiO_2 and TiO_2-graphene samples. The synergistic effect of chitosan and titanium dioxide by photodegradation technique was reported (Farzana and Meenakshi 2014) for the removal of toxic dyes and explained the synchronous role of chitosan and TiO_2 present in the system for both adsorption and photodegradation activities. Removal of nitrate ions by

Chitosan/Zeolite Y/Nano ZrO_2 nanocomposite as adsorbent was investigated (Teimouri et al. 2016), in which an adsorption capacity of 23.58 mg nitrate per g of the adsorbent was observed.

The present work deals with the development of a functional material based on chitosan and titanium dioxide in the form of beads that can remove nitrates from water/wastewater through an integrated adsorption cum photocatalysis technique enabled through a nanocomposite approach. Titanium dioxide doped with silver ions (Ag) acts as the photocatalyst for the reduction of nitrates while the adsorption of nitrates and other toxic elements in the aqueous solution is enabled by the porous structure of chitosan in the integrated nanocomposite system. Ag doping on titanium dioxide is envisaged to reduce the band gap energy of titanium dioxide thus making it active under visible light for practical applications. Further, the application of the synthesized nanocomposite beads in the removal of nitrates from model contaminated water was investigated in detail through batch/column adsorption cum photocatalytic studies under dark, UV, sunlight, and visible light.

An integrated adsorption cum photocatalytic removal of nitrates from water using bifunctional chitosan-titanium dioxide nanocomposite is not reported so far to the best of our knowledge. The novelty of the work relies on the fact that efficient removal of nitrates from water/wastewater using an integrated photocatalyst-adsorbent system derived from microwave-assisted sol-gel technique through a nanocomposite approach is rarely available in the literature. Thus, the novel integrated nanocomposite system developed in the present work offers superior functional features due to the synergistic effect of chitosan and titanium dioxide. The continuous flow fixed bed adsorption cum photocatalytic study performed using the functional material further suggests its potential for practical (domestic/industrial) applications in the field of water/wastewater treatment.

2. Experimental

2.1. Materials

Titanium(IV)tetraisopropoxide (97%) was procured from Sigma-Aldrich (U. S.) and was used as purchased. Glacial acetic acid (99%, Emplura), sodium hydroxide pellets, Glutaraldehyde (25%), Formic Acid (98–100%, Emparta→), and silver nitrate was supplied by Merck Life Science Pvt. Ltd., Mumbai, India. Chitosan (medium MW, extra pure with 90% deacetylated degree) was procured from Sisco Research Laboratories Pvt. Ltd, Maharashtra, India. Potassium nitrate (Emsure) was supplied by Sigma Aldrich, Germany.

2.2. Methods

2.2.1. Synthesis of silver doped TiO_2

The methodology for the synthesis of Ag-doped TiO_2 is schematically represented in Fig. S1. A single-step sol-gel methodology (Venkatachalam et al. 2007) is used for the synthesis of titanium dioxide sol in which titanium(IV)tetraisopropoxide (TTIP), glacial acetic acid, and water were mixed in the molar ratio of

1: 10: 350. In a typical experiment, to about 18.43 ml of TTIP, 35.57 ml of acetic acid was added and kept for stirring. To the solution under stirring, 390 ml of water is added slowly. The whole mixture was stirred for 1 hour and kept aside for 2 days when titania sol is formed. Silver doped titania was prepared by adding different quantities of $AgNO_3$ (0.5, 1, and 2 mol%) to 100 ml of the prepared titania sol. Silver nitrate added titania sols were then microwave heated in a kitchen microwave oven (600 W, frequency 50 Hz) for 5 minutes as depicted in Fig. S2. The synthesized Ag-doped titania was labelled as TA-0, TA-0.5, TA-1, and TA-2 where 'T' stands for titania and 'A' stands for Ag, and 0, 0.5, 1, and 2 stands for the mol% of $AgNO_3$ to that of titanium dioxide.

2.2.2. Synthesis of chitosan beads

Methodology for the synthesis of chitosan beads is schematically shown in Fig. S3. About 3g of the chitosan powder is mixed with 100 ml of 0.2 N acetic acid, followed by stirring for about 2 hours. This homogeneous solution is dropped into 50 ml of 0.5 N NaOH when chitosan hydrogel beads are obtained (Azlan et al. 2009). The size of the synthesized beads was found to depend on the nozzle size of the dropper. The beads were washed with distilled water until it reaches a neutral pH. The prepared beads were then cross-linked with glutaraldehyde solution (10%) by immersing in it for 24 hours followed by washing to get cross-linked chitosan beads.

2.2.3. Synthesis of Ag-doped TiO_2@chitosan beads

The synthesized chitosan beads are impregnated in the dispersion of microwave-treated Ag-doped titania sol for about 1 hour to get Ag-doped TiO_2 coated chitosan beads. The coated beads were then dried in a freeze dryer (Scanvac Cool Safe 55 – 4 Pro, -55°C) for 2 hours. Before freeze-drying, the samples were deep-frozen for 1 hour in a deep freezer (Blue star, 5°C). The synthesized Ag-doped titania coated chitosan beads were further labelled as CTA-0, CTA-0.5, CTA-1, and CTA-2 in which 'C' stands for chitosan, 'T' stands for titania, 'A' stands for Ag and 0, 0.5, 1 and 2 stands for the mol% of $AgNO_3$ to TiO_2. Coated beads of the sample CTA-0.5 was dried under oven condition also (65°C) to prepare oven-dried nanocomposite beads.

2.2.4. Characterizations

Undoped/Ag-doped titania and Ag-doped TiO_2@chitosan nanocomposite beads were characterized further using X-ray diffraction (XRD) analysis, Fourier Transform Infrared (FTIR) analysis, BET (Brunauer, Emmett and Teller) surface area measurements, UV-Visible Analysis, Field emission scanning electron microscopic (FESEM) analysis. BET surface area measurements and pore size analysis of the undoped and Ag-doped titania were carried out by nitrogen adsorption using a Micromeritics Gemini 2375 surface area analyzer after degassing each sample at 150–200°C for 2 hours. X-ray diffraction analysis of the powder samples was carried out in a PANALYTICAL, Aeris Research XRD instrument in the 2θ range 10–80° using Cu Kα radiation (λ = 1.54 Å). The Crystallite size of the anatase TiO_2 was calculated using the Debye-Scherer formula (Smitha et al. 2013).

$D_{XRD} = k\lambda/\beta Cos\theta$ (1)

where D_{XRD} is the average crystallite size, k has a value of 0.9 which is the shape factor, λ is the X-ray wavelength (1.5406 A˚ for Cu Kα1), β is the full width at half maximum of (1 0 1) peak and θ the Bragg angle.

The infrared spectrum of the nanocomposite beads was recorded in a Perkin Elmer Spectrum Two FTIR spectrometer, in the range 4000–400 cm^{-1} on the powder samples, using a Universal ATR accessory (UATR Two). UV-Visible spectra of TiO_2/Ag-doped TiO_2 were collected using a Cary 5000 UV-Vis-NIR spectrophotometer in the wavelength range 200–1000 nm. The morphology of the undoped and Ag-doped titania and that of pure chitosan, Ag-doped titania coated chitosan beads were observed using a Hitachi SU6600 Variable Pressure Field Emission Scanning Electron Microscope (FESEM) operated at 5kV.

2.2.5. Nitrate removal study using freeze-dried nanocomposite beads

The photocatalytic reduction of nitrates in the present study was followed by monitoring the concentration of nitrate anions in the presence of Ag-doped titania-coated chitosan beads under sunlight irradiation for 2 hours. About 1 g of the prepared nanocomposite beads were weighed in a beaker to which about 75 ml of the prepared nitrate solution (166 ppm) was added. (Potassium nitrate was used for preparing standard nitrate solution). Formic acid was added as a hole scavenger in the study to promote the photocatalytic nitrate reduction reaction. A molar ratio of 1:8 was followed between the nitrates and formic acid here. The whole solution under mild stirring was kept under dark conditions for about 30 minutes for equilibration. This equilibration time of 30 minutes given before the photocatalytic test is to eliminate the adsorption of nitrates by the porous chitosan network. 10 ml of the solution is withdrawn now which corresponds to the initial concentration of nitrate after nullifying the adsorption. The solution is then kept under sunlight exposure for about 2 hours. 10 ml of samples are withdrawn after 1, 2 hours under sunlight irradiation which corresponds to the concentration of nitrate at time intervals of 60, 120 minutes after sunlight exposure. The nitrate concentration was analyzed in a UV-Visible Spectrophotometer (Model: Evolution, Thermo Fischer) using the HCl method. The absorbance of the solutions was determined at λ_{max} = 270 nm. The quantity of nitrate remaining in the solution and the percentage removal of nitrate is calculated further using the equations given below. The concentration of the nitrate solution without the adsorbent was taken as the initial concentration (C_0). The concentration of the nitrate solutions at definite time intervals after adsorption/photocatalysis is taken as the final concentration (C). The concentration of nitrate remaining in the solution could be calculated from the formula as follows.

$Q = (C/C_0) *100$ (2)

where Q is the quantity of the nitrate remaining in %.

Similarly, the percentage removal of nitrate could be calculated using the equation given below.

$R = (C_0\text{-}C/C_0)*100$ (3)

where R is the % removal of nitrate.

2.2.6. Nitrate Removal Study using oven-dried nanocomposite beads

Removal of nitrates by the oven-dried chitosan beads/chitosan beads coated with Ag-doped TiO_2 (CTA-0.5) was also studied. Nitrate adsorption experiments under dark conditions were conducted using model water containing nitrate ions (100 ppm). The adsorption experiment was carried out by immersing 1 g of the nanocomposite beads into 75 ml of the standard nitrate solution, followed by stirring the solution using a magnetic stirrer. The experiment was conducted for about 180 minutes and 10 ml of the solution was collected at definite intervals of time (30 min). The nitrate concentration of the samples collected was measured using UV Visible spectrophotometer. The quantity of nitrate remaining and the percentage removal of nitrates was calculated using Equations (2) and (3) above.

Adsorption cum photocatalytic experiments were also conducted using the dried beads for the removal of nitrates from model contaminated water. Photocatalytic reduction of nitrates was followed by monitoring the concentration of nitrate anions in the presence of pure chitosan beads and Ag-doped titania coated chitosan beads under UV irradiation for 2 hours in a small UV chamber under constant stirring. The UV source was fourteen 8W UV-A tubes (354 nm) providing illumination of 755 lux. Stirring under dark conditions for about 1 hour was provided initially for the adsorption equilibration and the photocatalytic experiment was performed with and without the hole scavenger, formic acid. Nitrate concentrations of the solution at definite time intervals were measured as detailed above followed by calculating the percentage removal of nitrates.

2.2.7. Continuous flow fixed-bed column adsorption cum photocatalytic study using oven-dried nanocomposite beads

A continuous flow fixed bed column adsorption experiment was carried out further with the help of an experimental setup fabricated in-house. Figure 1. shows the photograph of the experimental setup fabricated in-house for the removal of nitrates from water.

The setup consisted of two acrylic glass columns of 2 cm internal diameter and height of 20 cm in which the nanocomposite beads are filled and model water containing nitrate ions is continuously passed through the columns at a definite flow rate using a peristaltic pump. The light source used was two Philips LED tube lights (15 W) that provides illumination in the visible region. Nitrate removal experiments were carried out under varying experimental conditions such as flow rate (5, 7.5, 10 $mlmin^{-1}$), bed height (6, 8, 12 cm corresponding to 12 g, 16 g and 24 g beads), and concentration of feed solution (100, 200

ppm). The experiments were performed in dark for 1 hour before switching on the visible light so that adsorption equilibration is attained. Photocatalytic experiments were performed for 2 hours of visible light exposure during which samples are collected at definite intervals and measured the nitrate concentration.

Representative fixed-bed column adsorption alone experiment was also carried out for the nitrate removal from a real groundwater sample. The column was packed to a height of 6 cm with 15 g beads as adsorbent on a layer of glass wool placed at the bottom of the column. Groundwater sample collected from Pallimukku, Palghat district, Kerala [Water quality parameters of the collected water sample are given in the Supplementary Information (Table SI).] with an initial nitrate concentration of 31.4 ppm was pumped through the column at a flow rate of 15 ml/minute. The water sample was collected from the exit of the column after 20 min for nitrate concentration and was analyzed using a UV visible Spectrophotometer.

The adsorbent capacity of the target nitrate ions was determined by the concentration before and after adsorption using Eq. 2.

$$qe = t.Q(C_{in} - C_{out})/m \quad (4)$$

where t is treatment time (h), Q is the flow rate (ml/min), C_{in} and C_{out} are the influent and effluent nitrate concentrations, respectively in mgl^{-1} and m is the total mass of adsorbent in the column (g).

The experiment was carried out under room temperature and data obtained was used to plot the graph from which nitrate removal efficiency was calculated.

3. Results And Discussion

The different processing stages involved in the synthesis of Ag-doped titania coated chitosan beads are presented below in Fig. 2. The color of the chitosan wet gel beads was found to change from white to brown after coating with Ag-doped titanium dioxide and freeze-drying for 1 hour. Pure chitosan beads after freeze-drying have shown less mechanical stability whereas the freeze-dried/oven-dried chitosan beads with Ag-doped titania coating have exhibited sufficient mechanical stability for handling. Silver doped titanium dioxide was characterized for its structural, textural, and morphological features and the results are presented below.

XRD analysis of undoped and Ag-doped titanium dioxide is presented in Fig. 3. XRD analysis of the Ag-doped TiO_2 shows the presence of phase pure anatase (JCPDS Card No: 00-021-1272) which is reported to be highly beneficial for the photocatalytic reduction of nitrate (Reyes-Coronado et al. 2008). No peaks corresponding to silver species were observed indicating that the addition is well below the doping level (below 2%) which is too low to show clear peaks.

Five minutes of microwave treatment of the synthesized titania sol (Peiró et al. 2001) and the silver doped titania sol has resulted in the crystallization of titanium dioxide in the anatase phase. Microwave heating of aqueous titania sol is reported to enhance the crystallization of titania as the presence of water as a solvent favors the crystallite formation (Smitha et al. 2013). Microwave energy is easily absorbed by polar solvents such as water resulting in homogeneous nucleation of the system due to the rapid energy transfer involved during the treatment. Kinetics of the crystallization of titania sol is significantly improved via the use of microwaves for a shorter duration (Dufour et al. 2012). Moreover, microwave energy facilitated the predominant growth of anatase crystallites suitable for photocatalytic application.

Figure 4 represents the morphological analysis of undoped titania and Ag-doped titania, microwave treated for five minutes. Nanosized titania particles are visible from the SEM images. The average particle size of titania was ~ 5–6 nm for undoped titania whereas it was ~ 3–4 nm for the 0.5 mol% Ag-doped titanium dioxide. TEM analysis of the TA-0.5 sample also shows the presence of anatase TiO_2 with a particle size as small as 3–4 nm. Particle sizes obtained from the SEM/TEM analysis were consistent with the crystallite sizes calculated from the XRD analysis for the anatase crystals using the Debye Sherrer Equation as the values were 5.4 nm and 4.8 nm for the undoped titania and Ag-doped titania (TA-0.5) respectively.

Reduction in the particle size of titanium dioxide to Ag doping is already reported in the literature which is ascribed to the decrease in the particle nucleation during hydrolysis/condensation of Ti(IV)isopropoxide in presence of silver species (Mogal et al. 2014). According to the researchers, there exists a critical Ag concentration above which the particle size increases (Li et al. 2020). Figure 5 presents the N_2 adsorption-desorption isotherms and the pore size distribution of the pure titania and the silver doped titania. A type IV isotherm with a hysteresis loop characteristic of the mesoporous materials was obtained from the surface area analysis (Sotomayor et al. 2018). Pure titania had a surface area of 251 m^2g^{-1} (Table I). Among the different samples, TA-0.5 has shown the highest surface area of 282 m^2g^{-1}. There was only a marginal increase in the surface area for the 1 mol% Ag-doped sample when compared to the undoped sample and it was found to decrease further by increasing the percentage doping. The fine mesoporous structure of the titanium dioxide and Ag-doped titanium dioxide as evident from a monomodal pore size distribution is also very clear in Fig. 5b. TA-0.5 has shown a narrow pore size distribution when compared to that of other samples.

Table I. Textural features of titania and Ag doped titania, microwave treated for 5 minutes.

Sample	BET Surface Area (m^2g^{-1})	Total Pore Volume (cm^3g^{-1})	Micropore Volume (cm^3g^{-1})	Mesopore Volume (cm^3g^{-1})	Pore diameter (nm)
TA-0	251.4	0.3043	-0.0195	0.3238	4.8
TA-0.5	282.3	0.3150	-0.0131	0.3281	4.5
TA-1	253.6	0.2904	-0.0178	0.3082	4.6
TA-2	227.8	0.3343	-0.0123	0.3466	4.7

The high surface area of the TA-0.5 sample obtained here could be due to the reduction in the crystallite size due to the effective doping by the Ag ions. The Ag ions existing on the surface of anatase titania particles can hinder the mutual contact and material transfer between the anatase grains, thereby depressing the grain growth of anatase leading to an increased surface area (Chao et al. 2003).

The UV-Visible absorbance of pure titanium dioxide and TA-0.5 was further recorded using a UV-Visible spectrophotometer and the obtained results are presented in Fig. S5. Absorption in the visible region (400–800 nm) was more for Ag-doped titania when compared to that of pure titania indicating that Ag-doped TiO_2 may be active under visible light irradiation (Li et al. 2011).

Figure 6 represents the FTIR analysis of the undoped titania coated chitosan beads and the 2 mol% Ag-doped titania coated chitosan beads. FTIR spectra mainly show the vibrational modes of chitosan in the undoped and Ag-doped systems (de Souza et al. 2015). The broad band centered at 3300 cm^{-1} shows the overlapping of O-H and N-H stretching vibration, together with N-H secondary amine stretching of the cross-linked chitosan. The presence of bands corresponding to amides was noted at 1633 cm^{-1} and 1550 cm^{-1}. The band at 1026 cm^{-1} and 1072 cm^{-1} is attributed to the C–O stretching vibration contributed by the primary alcohol in chitosan. Bands corresponding to CH_2 bending and C-O-C asymmetric stretching vibration were also observed at 1411 and 1155 cm^{-1} respectively. Ag-doped TiO_2-coated chitosan beads contain a trace amount of silver oxide in them. The different peaks obtained from the FTIR spectra are assigned to their respective vibrational modes as given in Table II.

Both the samples had characteristic Ti-O-Ti stretching vibration for TiO_2 at 410 cm^{-1} (Vasconcelos et al. 2011) whereas TA-2 coated chitosan beads contain a small peak at 455 cm^{-1} corresponding to the presence of oxidized silver species (Ag_2O) (Pawar et al. 2016).

Table II. FTIR peak assignment (de Souza et al. 2015) for TA-0 and TA-2 coated chitosan beads, freeze-dried for 1 hour.

No.	FTIR peak (cm^{-1})	Vibrational Mode	Assignment
a	3220–3380	NH & OH Stretching	Amines & H_2O
b	1633	N-H bending vibration	Secondary amide
c	1550	N-H bending vibration	Secondary amide
d	1411	CH_2 bending	Pyranose ring
e	1155	C-O-C asymmetric stretching	from β(1–4) bond
f	1072	C-O stretching	Primary OH
g	1026	C-O stretching	Primary OH
h	410 cm^{-1}	(Ti-O-Ti) stretching vibration	TiO_2

Other vibrational peaks obtained for NH, OH, CH_2, CO, etc. are characteristic of the chitosan polymer which is present in both the samples. Thus, FTIR analysis revealed the successful formation of the chitosan-titania nanocomposite as evidenced by the characteristic peaks corresponding to the chitosan and titanium dioxide.

SEM analysis of the pure chitosan beads and the 0.5 mol% Ag doped titania coated chitosan beads, after freeze-drying for 1 hour is presented in Fig. 7.

The microporous structure of the prepared chitosan beads is very clear from the SEM images with an average pores size of ~ 0.5 mm. Ag-doped TiO_2 gets coated uniformly over the porous surface of chitosan which eventually decreases the pores size of chitosan (Jayakumar et al. 2011) from ~ 0.5 mm to ~ 0.25 mm. TA-0.5 coated chitosan beads have shown hard agglomerates on the surface of the beads could be due to the presence of excess TiO_2 that gets precipitated out.

The photocatalytic reduction of nitrates by the freeze dried nanocomposite beads was monitored by measuring the concentration of nitrate ions in the model water sample (spiked with nitrate ions) subjected to photocatalytic studies under sunlight for 2 hours in the presence of a hole scavenger. Undoped titania and Ag-doped titania coated chitosan beads were subjected to a photocatalytic reduction study. The nitrate solution along with the coated chitosan beads was kept in the dark for about half an hour to nullify the effect of any adsorption by the porous structured chitosan beads. Table III provides the adsorption and photocatalytic efficiency of the synthesized chitosan beads with varying Ag concentrations towards nitrate anion. The obtained results clearly shows that Ag doping on titania is affecting the adsorption characteristics of the synthesized chitosan beads. The sample, CTA-0.5, the one containing 0.5 mol% Ag-doped titania coated chitosan beads are showing a nitrate adsorption efficiency of 43.5%. The smaller particle size (~ 10 nm) and enhanced surface area of the TA-0.5 sample might have contributed to the relatively high adsorption efficiency (Tian et al. 2008). About 95% nitrate

reduction efficiency was observed for the sample CTA-0.5 which was the highest efficiency among the other samples. Undoped titania-coated chitosan beads had a nitrate reduction efficiency of 42%.

Table III. Adsorption efficiency of the undoped and Ag-doped titania coated chitosan beads towards nitrates.

Sample	Initial nitrate concentration (ppm)	Remaining nitrate after adsorption (ppm)	Adsorption efficiency (%)	Photocatalytic efficiency (%)
CTA-0	166	100.9	39.2	42
CTA-0.5	166	93.7	43.5	95
CTA-1	166	100.7	39.3	37
CTA-2	166	93.4	43.7	80

According to the researchers, many factors such as particle size of titanium dioxide, reaction temperature, the metal used for doping, and hole scavenger and its concentration can influence the photocatalytic nitrate reduction efficiency. The hole scavenger formic acid used in the study aids in achieving significantly higher nitrate conversion (Doudrick et al. 2013). A decrease in the particle size of titanium dioxide due to the Ag doping in the present work increases the amount of exposed unit area per unit mass which increases the adsorption efficiency. The metal species (Ag) clusters incorporated on the TiO_2 surface can induce the formation of oxygen vacancies which act as electron traps (Pan et al. 2013). The new allowed electronic states below the TiO_2 conduction band enhance the visible light absorption of the photocatalysts which makes them active even under sunlight due to the band gap energy modification. Moreover, the new energy levels created can act as an electron sink, which improves the electron-hole separation and thus more electrons will be available on the catalyst surface for the nitrate reduction reaction (Sa et al. 2009). The UV-visible absorbance spectra of pure TiO_2, Ag doped TiO_2 and the mechanism behind the photocatalytic nitrate reduction (Kobwittaya and Sirivithayapakorn 2014) is presented in Fig. 8.

It is assumed that the end product of the nitrate reduction reaction in the present work is N_2 as no nitrites were measured during the ion chromatographic (IC) analysis of the samples collected and there was no significant change in the pH of the sample out of NH^{4+} ions. Thus, in the present work, Ag-doped TiO_2 coated chitosan beads (CTA-0.5) show superior nitrate reduction efficiency and adsorption efficiency which makes it a suitable candidate for the removal of nitrates from water/wastewater. The nanocomposite CTA-0.5 was selected for further studies considering its high adsorption as well as photocatalytic efficiency towards the removal of nitrate from water.

Figure 9 represents the surface morphology of oven-dried pure chitosan beads and Ag-doped TiO_2 coated chitosan (CTA-0.5) beads. The porous structure of the chitosan bead was considerably changed for the oven-dried sample when compared to that of the freeze-dried sample. The pore size of the pure chitosan

beads was in the range of 50–100 nm whereas the mesoporous structure of the chitosan beads was uniformly covered with nanoparticles of titanium dioxide with a size less than 10 nm as revealed from Fig. 9b-c.

Batch/column adsorption cum photocatalytic experiments were also carried out using the CTA-0.5 nanocomposite beads in its oven dried form as it exhibits more mechanical stability when compared to the freeze dried sample. Results on the nitrate adsorption study of pure chitosan beads and CTA-0.5 beads (oven dried) under dark conditions are presented below in Fig. 10a. From the results, it is clear that Ag-doped TiO_2 coating over the chitosan beads significantly increases the adsorption efficiency of the beads, and the adsorption of nitrates is getting saturated within 1 hour of stirring under dark conditions as major concentration changes of nitrates was not observed further. Figure 10b demonstrates the adsorption cum photocatalytic efficiency of the oven dried chitosan beads coated with Ag-doped TiO_2 in removing nitrates from model contaminated water.

The adsorption efficiencies were 10.9% and 54–60% for the pure chitosan beads and Ag-doped TiO_2 coated chitosan beads respectively under dark stirring conditions for 1 hour. The photocatalytic efficiencies were ~ 8.8% for pure chitosan beads whereas it was 70%, 69% and 53% for Ag-doped TiO_2 coated chitosan beads with nitrate: formate ratio 1:2, 1:5 and 1:8 respectively in 2 hours of UV irradiation time. Pure chitosan beads lack photocatalytic activity while an enhanced photocatalytic efficiency of the nanocomposite system was observed in the presence of formic acid scavenger.

When the nanocomposite is irradiated with incident light having energy greater than the band gap of titanium dioxide, electrons and holes are generated that can be utilized for the reduction and oxidation, respectively. However, the recombination of the electron and holes in a few nanoseconds can slow down the redox reactions on the surface of the semiconductor and hence adding a hole scavenger (i.e., electron donor) can help overcome the recombination effect and provide a continuous supply of electrons for the nitrate reduction reaction. Formic acid scavenger is reported to have highest activity among other scavengers and the overall redox reaction between nitrate and formic acid with TiO_2 under UV irradiation could be represented as given below when the formate: nitrate ratio is 1:2.5 (Yang et al. 2013).

$$2NO^{3-} + 5HCOOH + 2H^{+} \rightarrow N_2 + 5CO_2 + 6H_2O \quad (5)$$

During nitrate reduction reaction, both formic acid and nitrate will get consumed and an ideal stoichiometric ratio of 2.5 between the formate and nitrate is considered to offer 100% N_2 selectivity. The photocatalytic efficiencies were nearly same when the nitrate:formate ratio was 1:2 to 1:5 in the present study and the formic acid scavenger helps in attaining significantly higher nitrate conversion as it can abstract the holes thereby making more electrons available for the nitrate reduction reaction.

Figure 11 demonstrates the results on the continuous flow adsorption cum photocatalytic studies of the nanocomposite beads carried out in an experimental set up fabricated in-house. Figure 11a shows the effect of the integrated adsorbent-cum photocatalyst system in reducing the nitrate levels well below the

permissible limits of standard drinking water in a fixed bed continuous flow system even up to 5 hours whereas the nitrate levels increase above the permissible limits in 200 min itself if we are exploring only the adsorption property of the material. Figure 11b-c shows that as the bed height of the column increases from 6 to 12 cm, there is a prominent effect on the nitrate removal characteristics and nitrate removal for a longer time can be enabled by increasing the bed height to a desired level. The nitrate removal percentage is increased from 49.6–60.8% and to 97.5% when the bed height is increased from 6 cm, 8 cm and to 12 cm in 5 hours time. A larger amount of nitrate gets adsorbed when the bed height is high due to an increase in the surface area of adsorbent cum photocatlyst, providing more binding sites for the adsorption, followed by photocatalytic removal.

The effect of concentration was also studied using continuous flow adsorption cum photocatalysis study in the fabricated water treatment set up that shows a nitrate removal efficiency of 87.6% & adsorption capacity 7.9 mgg^{-1} for 8 hours when using an inlet concentration of 100 ppm for a bed height of 12 cm at 5.0 $mlmin^{-1}$ flow rate. The nitrate removal efficiency was 55.5% with an adsorption capacity of 7.3 mgg^{-1} for 5 hours when using an inlet concentration of 250 ppm for a bed height of 12 cm at 5.0 ml/min flow rate.

In summary, the variations in the residual nitrate are prominent when the amount of catalyst is low and at higher initial concentration of nitrate, and at high flow rate conditions, indicating the need for scavenger addition at a minimum level for a higher overall nitrate removal efficiency in the continuous flow system of adsorption cum photocatalysis. Considering the relatively high adsorption efficiency of the synthesized functional nanocomposite beads, a column adsorption alone experiment was also performed and the results obtained for the adsorption of various anions from a real groundwater sample are presented below in Table IV.

Table IV: Results of the column adsorption study using functional nanocomposite beads.

Sample	Anions	Initial concentration (ppm)	Concentration after adsorption for 20 min (ppm)	Adsorption efficiency (%)
Pure chitosan bead-	Nitrate	31.4	15.4	50.8
CTA-0.5 bead	Nitrate	31.4	4.4	85.9
Pure chitosan bead	Sulphate	29.0	27.0	6.9
CTA-0.5 bead	Sulphate	29.0	1.0	96.5
Pure chitosan bead	Phosphate	0.84	2.9	---
CTA-0.5 bead	Phosphate	0.84	0.81	3.6
Pure chitosan bead	Chloride	127.9	121.9	4.7
CTA-0.5 bead	Chloride	127.9	51.9	59.4

It was found that the synthesized functional nanocomposite beads are highly efficient in the removal of nitrates and other anions present in a real groundwater sample when compared to that pure chitosan beads. The mechanism behind the removal of nitrates and other anions is attributed to the electrostatic attraction by the positively charged TiO_2 coated chitosan beads. Thus, the efficiency of the functional nanomaterial synthesized in the present work for the removal of multiple ions from groundwater samples suggests the potential of the material for water/wastewater filtration application.

4. Conclusions

Ag-doped titania coated chitosan beads were successfully synthesized by a sol-gel method in the present work. Microwave treatment of the synthesized titania sol and the silver doped titania sol has resulted in the crystallization of titanium dioxide preferably in the anatase phase which is the highly photoactive phase. A reduction in the particle size of titanium dioxide was observed in Ag doping which is ascribed to the decrease in the particle nucleation during hydrolysis/condensation of the titania precursor in the presence of silver species. The synthesized Ag-doped titania (TA-0.5) has enhanced surface area and narrow pore size distribution when compared to that of undoped titania. Ag-doped TiO_2 gets coated uniformly over the porous surface of chitosan which eventually decreases the pore size of chitosan from ~ 0.5 mm to ~ 0.25 mm. The freeze-dried chitosan-titania nanocomposite beads containing 0.5 mol% Ag exhibited an adsorption efficiency of ~ 43.5% (under dark for 30 min) and photocatalytic reduction capability of ~ 95% (under sunlight for 2 hours), whereas the adsorption and photocatalytic efficiencies

were 40% (under dark for 30 min) and 70% (under UV light for 2 hours) respectively, in the case of oven-dried nanocomposite beads, towards the removal of nitrate ions in an aqueous solution. A nitrate removal efficiency of 87.6% and an adsorption capacity of 7.9 mgg^{-1} were obtained for the nanocomposite beads in the continuous flow adsorption cum photocatalysis experiment for up to 8 hours when using an inlet concentration of 100 ppm, bed height 12 cm and flow rate 5.0 $mlmin^{-1}$. Fixed bed column adsorption alone experiment also shows promising results for a real groundwater sample with 85.9% nitrate removal efficiency. Thus, the superior nitrate removal efficiency of the Ag doped TiO_2 coated chitosan beads via adsorption/photocatalysis make it a suitable candidate for the removal of nitrates from contaminated water using adsorption/photocatalysis.

Declarations

Acknowledgements

The authors acknowledge the Executive Director, CWRDM, for providing the facilities to carry out the research work. Ms. Arathi AR and Ummu Habeeba are being acknowledged for the work carried out as part of their dissertation work. Acknowledgment is due to Dr. Jayasooryan KK for groundwater sampling, Mr. Peer Mohammed A, CSIR-NIIST, Trivandrum, for the BET Surface Area Analysis. All the members of Ecology and Environment Research Group, CWRDM, are being acknowledged for providing general assistance.

Author contribution

The concept of this study was developed by SVS. The experimental work was carried out by AP with guidance from SVS. VT conducted the groundwater sampling. SVS drafted the article. HPS and RTR were involved in the critical revision of the article. All the authors read and approved the final manuscript.

Funding sources

This work was funded by Kerala State Government Plan Fund, CWRDM.

Availability of data and materials

The datasets used and/or analyzed during the current study are available from the corresponding author on reasonable request.

Ethics approval and consent to participate - Not applicable.

Consent for publication - Not applicable.

Competing interests - The authors declare no competing interests.

References

1. Archna SK, Sharma RC, Sobti (2012) Nitrate Removal from Ground Water: A Review. J. Chem. 9:154616.
2. Azlan K, Wan Saime WN, Lai Ken L (2009) Chitosan and chemically modified chitosan beads for acid dyes sorption. J. Environ. Sci. 21:296-302.
3. Banu HAT, Karthikeyan P, Meenakshi S (2021) Removal of nitrate and phosphate ions from aqueous solution using zirconium encapsulated chitosan quaternized beads: Preparation, characterization and mechanistic performance. Results in Surfaces and Interfaces, 3:100010.
4. Chao HE, Yun YU, Xingfang HU, Larbot A (2003) Effect of silver doping on the phase transformation and grain growth of sol-gel titania powder. J. Eur. Ceram. 23:1457-1464.
5. Dahab MF (1991) Nitrate Treatment Methods: An Overview, in: I. Bogárdi, R.D. Kuzelka, W.G. Ennenga (Eds.) Nitrate Contamination. Springer Berlin Heidelberg, Berlin, Heidelberg, pp. 349-368.
6. de Souza NLG, Salles T, Brandao H, Edwards H, De Oliveira LF (2015) Synthesis, Vibrational Spectroscopic and Thermal Properties of Oxocarbon Cross-Linked Chitosan. J. Braz. Chem. Soc. 26: 1247-1256.
7. Doudrick K, Monzón O, Mangonon A, Hristovski K, Westerhoff P (2012) Nitrate Reduction in Water Using Commercial Titanium Dioxide Photocatalysts (P25, P90, and Hombikat UV100). J. Environ. Eng. 138:852-861.
8. Doudrick K, Yang T, Hristovski K, Westerhoff P (2013) Photocatalytic nitrate reduction in water: Managing the hole scavenger and reaction by-product selectivity. Appl. Catal. B 136-137:40-47.
9. Dufour F, Cassaignon S, Durupthy O, Colbeau-Justin C, Chanéac C (2012) Do TiO_2 Nanoparticles Really Taste Better When Cooked in a Microwave Oven?. Eur. J. Inorg. Chem. 2012:2707-2715.
10. Farzana MH, Meenakshi S (2014), Synergistic Effect of Chitosan and Titanium Dioxide on the Removal of Toxic Dyes by the Photodegradation Technique. Ind. Eng. Chem. Res. 53:55-63.
11. Huno SKM, Rene ER, van Hullebusch ED, Annachhatre AP (2018) Nitrate removal from groundwater: a review of natural and engineered processes. J. Water Supply Res. T. 67:885-902.
12. Jayakumar R, Ramachandran R, Divyarani VV, Chennazhi KP, Tamura H, Nair SV (2011) Fabrication of chitin–chitosan/nano TiO_2-composite scaffolds for tissue engineering applications. Int. J. Biol. Macromol. 48 :336-344.
13. Kobwittaya K, Sirivithayapakorn S (2014) Photocatalytic reduction of nitrate over TiO_2 and Ag-modified TiO_2. J. Saudi Chem. Soc. 18:291-298.
14. Li D, Song H, Meng X, Shen T, Sun J, Han W, Wang X (2020) Effects of Particle Size on the Structure and Photocatalytic Performance by Alkali-Treated TiO_2. Nanomaterials 10:546.
15. Li Y, Ma M, Chen W, Li L, Zen M (2011) Preparation of Ag-doped TiO_2 nanoparticles by a miniemulsion method and their photoactivity in visible light illuminations. Mater. Chem. Phys. 129:501-505.
16. Liu Z, Rui M, Yu S (2022) Occurrence of titanium dioxide nanoparticle in Taihu Lake (China) and its removal at a full-scale drinking water treatment plant. Environ. Sci. Pollut. Res. 29:23352-23360.

17. Marcelino RBP, Amorim CC (2019) Towards visible-light photocatalysis for environmental applications: band-gap engineering versus photons absorption—a review. Environ. Sci. Pollut. Res. 26:4155-4170.
18. Mehran, A, AghaKouchak A, Nakhjiri N, Stewardson MJ, Peel MC, Phillips TJ, Wada Y, Ravalico JK, (2017) Compounding Impacts of Human-Induced Water Stress and Climate Change on Water Availability Sci. Rep. 7:6282.
19. Mogal SI, Gandhi VG, Mishra M, Tripathi S, Shripathi T, Joshi PA, Shah DO (2014) Single-Step Synthesis of Silver-Doped Titanium Dioxide: Influence of Silver on Structural, Textural, and Photocatalytic Properties. Ind. Eng. Chem. Res. 53:5749-5758.
20. Mohammadi R, Sabourmoghaddam N (2020), TiO_2-graphene/chitosan nanocomposite: preparation and its application for removal of anionic dyes. Asian J. Green Chem. 4:11-32.
21. Mohsenipour M, Shahid S, Ebrahimi K (2014) Removal Techniques of Nitrate from Water. Asian J. Chem. 26:7881-7886.
22. Pan X, Yang MQ, Fu X, Zhang N, Xu YJ (2013) Defective TiO_2 with oxygen vacancies: synthesis, properties and photocatalytic applications. Nanoscale 5:3601-3614.
23. Pawar O, Deshpande N, Dagade S, Waghmode S, Nigam Joshi P (2016) Green synthesis of silver nanoparticles from purple acid phosphatase apoenzyme isolated from a new source. Limonia acidissima, J. Exp. Nanosci. 11:28-37.
24. Peiró AM, Peral J, Domingo C, Domènech X, Ayllón JA (2001) Low-Temperature Deposition of TiO_2 Thin Films with Photocatalytic Activity from Colloidal Anatase Aqueous Solutions. Chem. Mater. 13:2567-2573.
25. Reyes-Coronado D, Rodríguez-Gattorno G, Espinosa-Pesqueira ME, Cab C, de Coss R, Oskam G (2008) Phase-pure TiO_2 nanoparticles: anatase, brookite and rutile. Nanotechnology 19:145605.
26. Sá J, Agüera CA, Gross S, Anderson JA (2009) Photocatalytic nitrate reduction over metal modified TiO_2. Appl. Catal. B 85:192-200.
27. Shukla S, Saxena A (2019) Global Status of Nitrate Contamination in Groundwater: Its Occurrence, Health Impacts, and Mitigation Measures, in: C.M. Hussain (Ed.) Handbook of Environmental Materials Management. Springer International Publishing, Cham, pp. 869-888.
28. Silva CG, Pereira MFR, Órfão JJM, Faria JL, Soares OSGP (2018) Catalytic and Photocatalytic Nitrate Reduction Over Pd-Cu Loaded Over Hybrid Materials of Multi-Walled Carbon Nanotubes and TiO_2. Front. Chem. 6:632.
29. Smitha VS, Jaimy KB, Shajesh P, Jeena JK, Warrier KG (2013) UV curable hydrophobic inorganic–organic hybrid coating on solar cell covers for photocatalytic self cleaning application. J. Mater. Chem. A 1:12641-12649.
30. Smitha VS, Jyothi CK, Mohamed AP, Pillai S, Warrier KG (2013) Novel multifunctional titania–silica–lanthanum phosphate nanocomposite coatings through an all aqueous sol–gel process. Dalton Trans. 42:4602-4612.

31. Sotomayor F, Cychosz K, Thommes M (2018) Characterization of Micro/Mesoporous Materials by Physisorption: Concepts and Case Studies. Acc. Mater. Surf. Res. 3:34-50.
32. Szymańska E, Winnicka K (2015) Stability of chitosan-a challenge for pharmaceutical and biomedical applications. Mar. Drugs 13:1819-1846.
33. Teimouri A, Nasab SG, Vahdatpoor N, Habibollahi S, Salavati H, Chermahini AN (2016) Chitosan /Zeolite Y/Nano ZrO_2 nanocomposite as an adsorbent for the removal of nitrate from the aqueous solution. Int. J. Biol. Macromol. 93:254-266.
34. Tian G, Fu H, Jing L, Xin B, Pan K (2008) Preparation and Characterization of Stable Biphase TiO_2 Photocatalyst with High Crystallinity, Large Surface Area, and Enhanced Photoactivity. J. Phys. Chem. C 112:3083-3089.
35. Vasconcelos DCL, Costa VCo, Nunes EHM, Sabioni AnCS, Gasparon M, Vasconcelos WL (2011) Infrared Spectroscopy of Titania Sol-Gel Coatings on 316L Stainless Steel, Materials Sciences and Applications. 2:1375-1382.
36. Venkatachalam N, Palanichamy M, Murugesan V (2007) Sol–gel preparation and characterization of nanosize TiO_2: Its photocatalytic performance. Mater. Chem. Phys. 104:454-459.
37. Ward MH, Jones RR, Brender JD, de Kok TM, Weyer PJ, Nolan BT, Villanueva CM, van Breda SG (2018) Drinking Water Nitrate and Human Health: An Updated Review. Int. J. Environ. Res. Public Health 15:1557.
38. Yang T, Doudrick K, Westerhoff P (2013) Photocatalytic reduction of nitrate using titanium dioxide for regeneration of ion exchange brine. Water Res. 47:1299-1307.
39. Zarei S, Farhadian N, Akbarzadeh R, Pirsaheb M, Asadi A, Safaei Z (2020) Fabrication of novel 2D Ag-TiO_2/γ-Al_2O_3/Chitosan nano-composite photocatalyst toward enhanced photocatalytic reduction of nitrate. Int. J. Biol. Macromol. 145: 926-935.

Figures

Figure 1

Photograph of the experimental setup that was fabricated in-house, used for the continuous flow adsorption cum photocatalytic study.

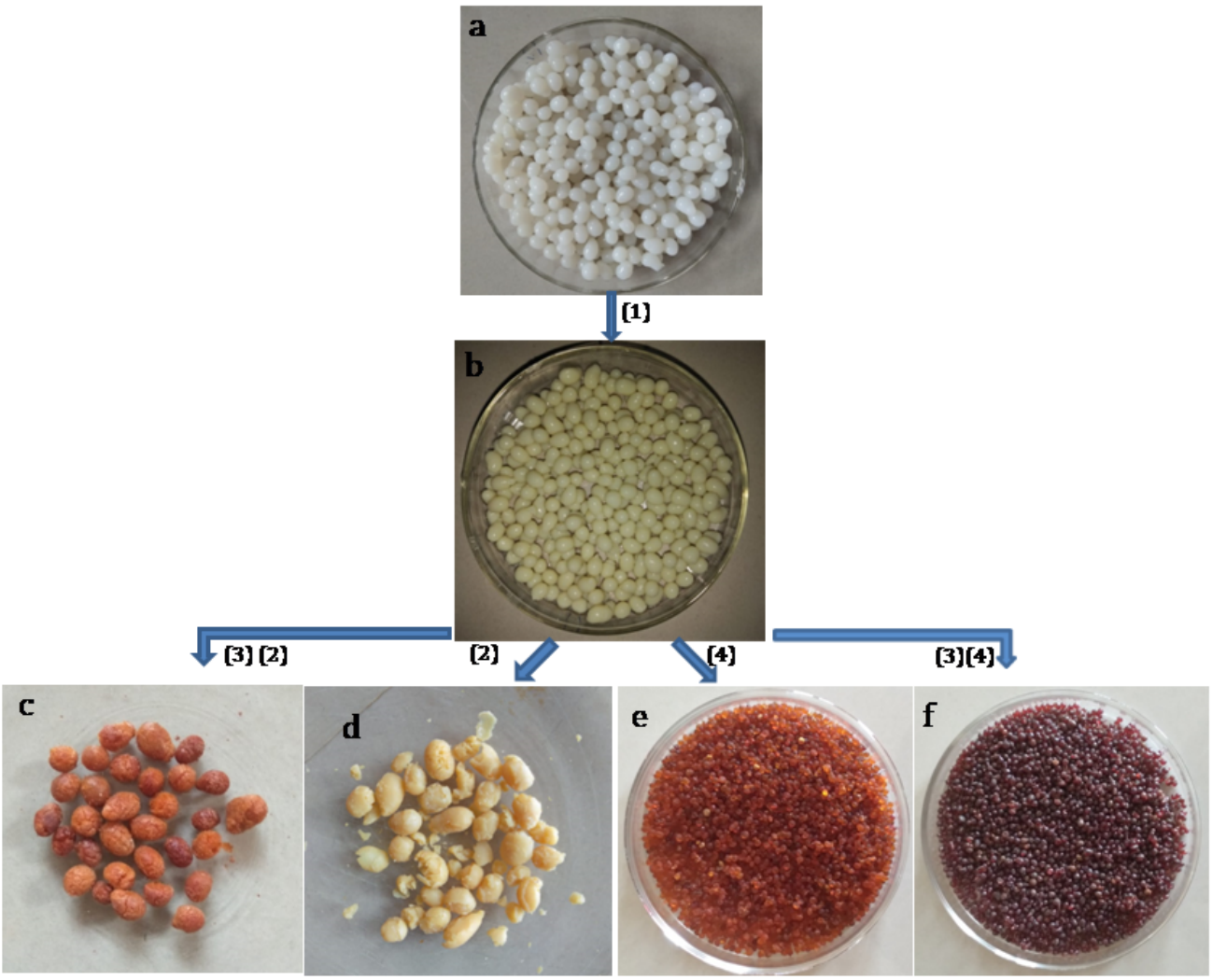

Figure 2

Synthesis of Ag-doped titania coated chitosan beads through different stages (a) pure chitosan beads (b) crosslinked chitosan beads (c) freeze-dried crosslinked chitosan beads and (d) Freeze-dried, Ag-doped TiO2coated crosslinked chitosan beads (e) Oven-dried crosslinked chitosan beads and (f) Oven-dried, Ag-doped TiO2 coated crosslinked chitosan beads [Different stages involved in the processing are (1) crosslinking by impregnation in 10% glutaraldehyde solution (2) freeze-drying for 1h (3) impregnation in Ag-doped titania sol (4) oven drying for 24 h]

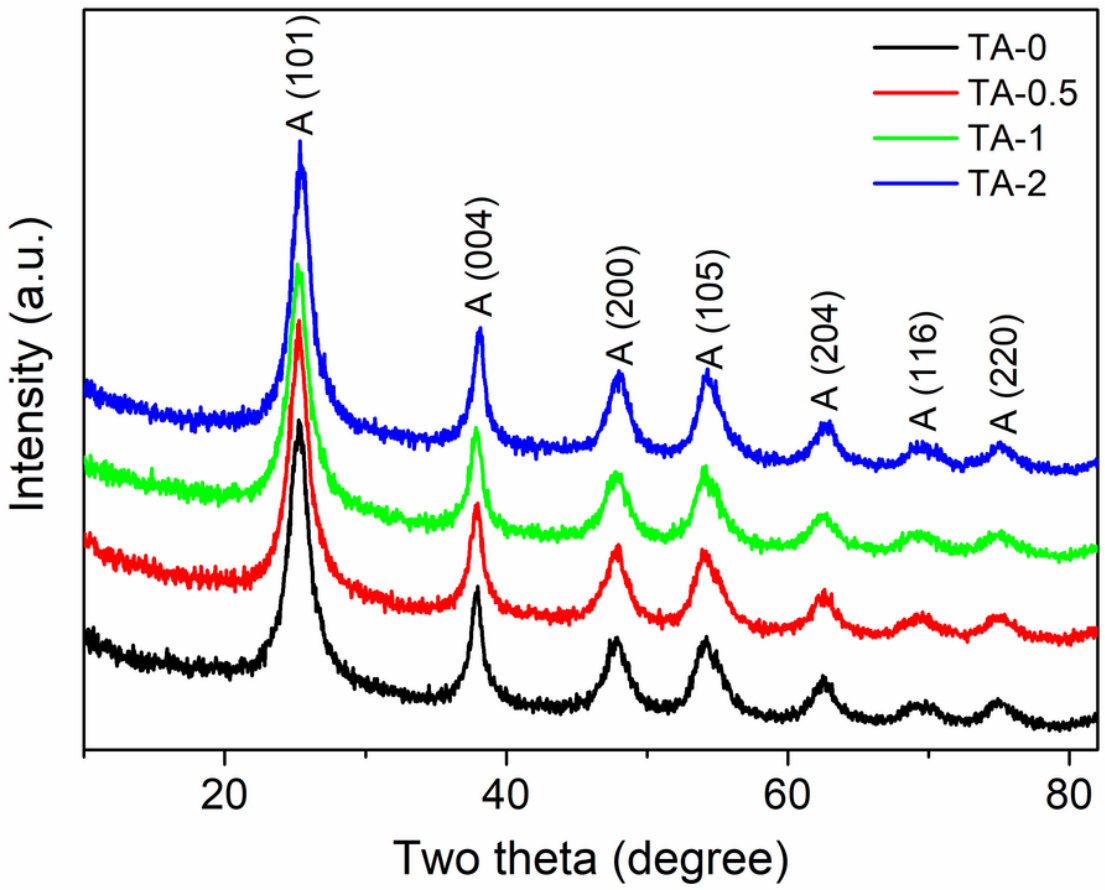

Figure 3

X-ray diffraction patterns for titanium dioxide and Ag doped titania.

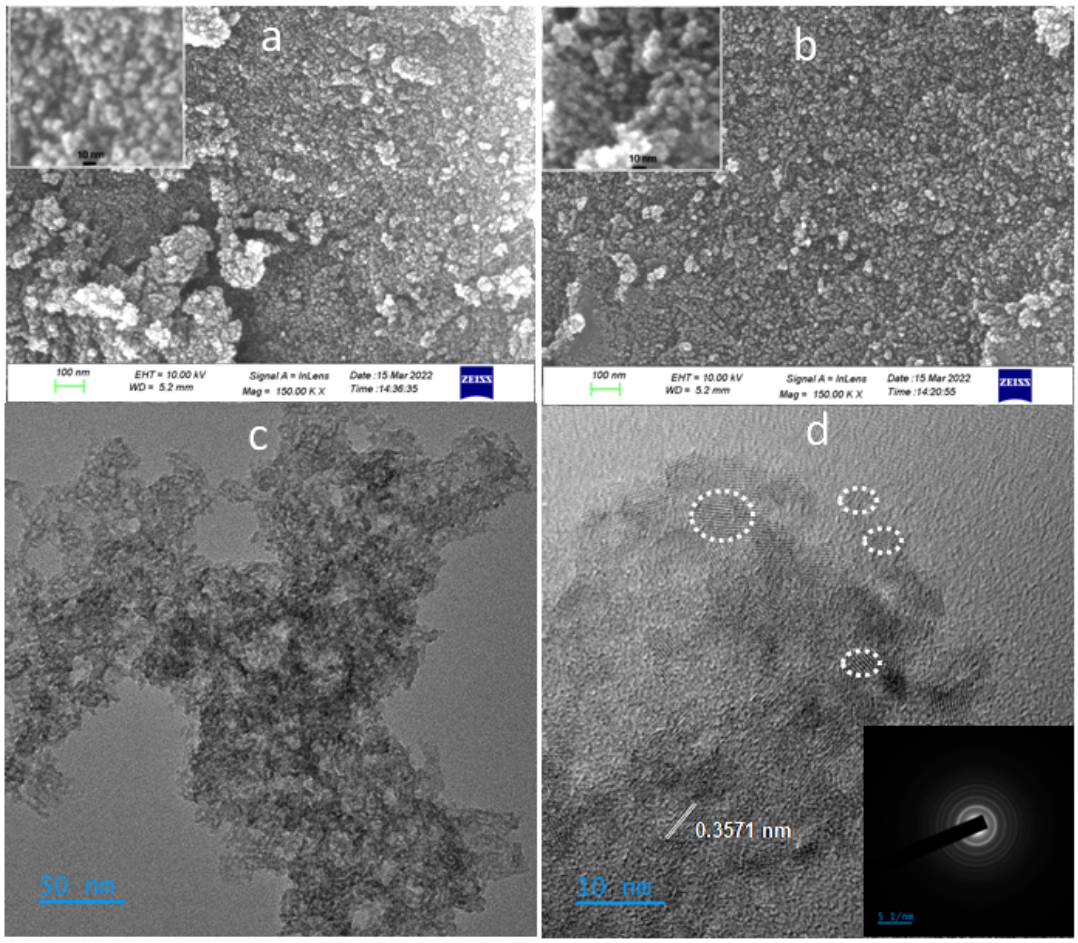

Figure 4

SEM analysis of (a) undoped titanium dioxide, (b) 0.5 mol% Ag-doped titanium dioxide, both microwave treated for 5 minutes (zoomed images are provided as inset), and TEM analysis of (c) 0.5 mol% Ag-doped titanium dioxide, microwave treated for 5 minutes, (d) High-resolution image of ‘c’ with SAED pattern in the inset.

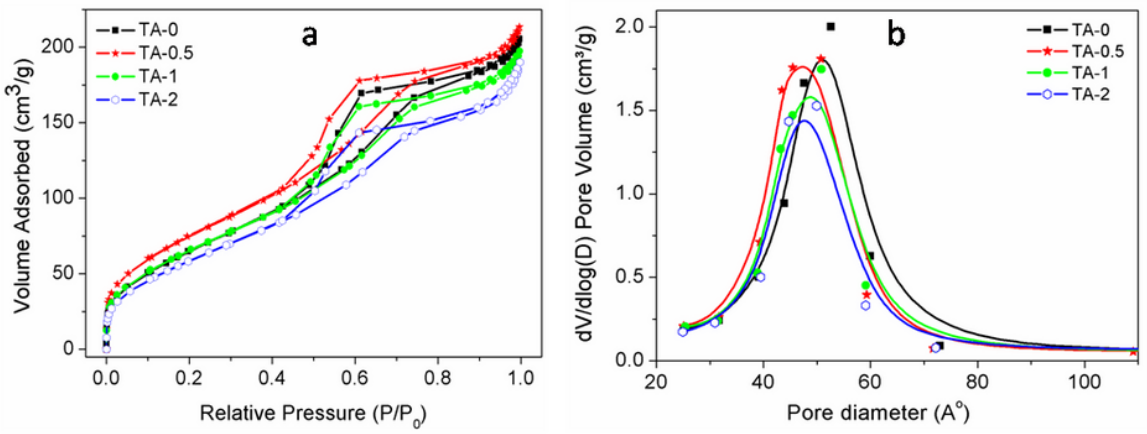

Figure 5

(a) Adsorption-desorption isotherms and (b) pore size distribution of pure titania and Ag-doped titania, microwave treated for five minutes.

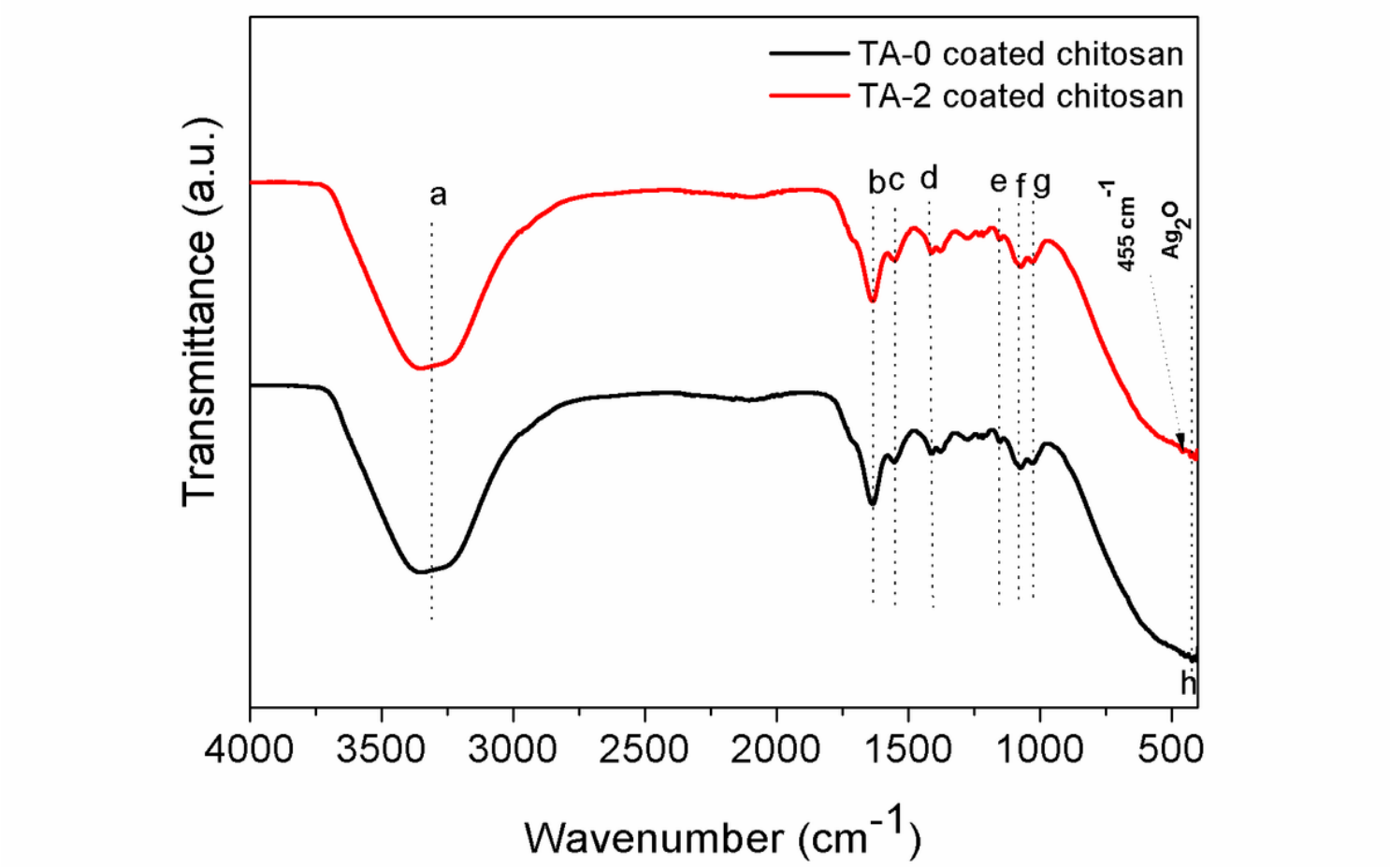

Figure 6

FTIR analysis of TA-0 and TA-2 coated chitosan beads freeze-dried for 1 hour.

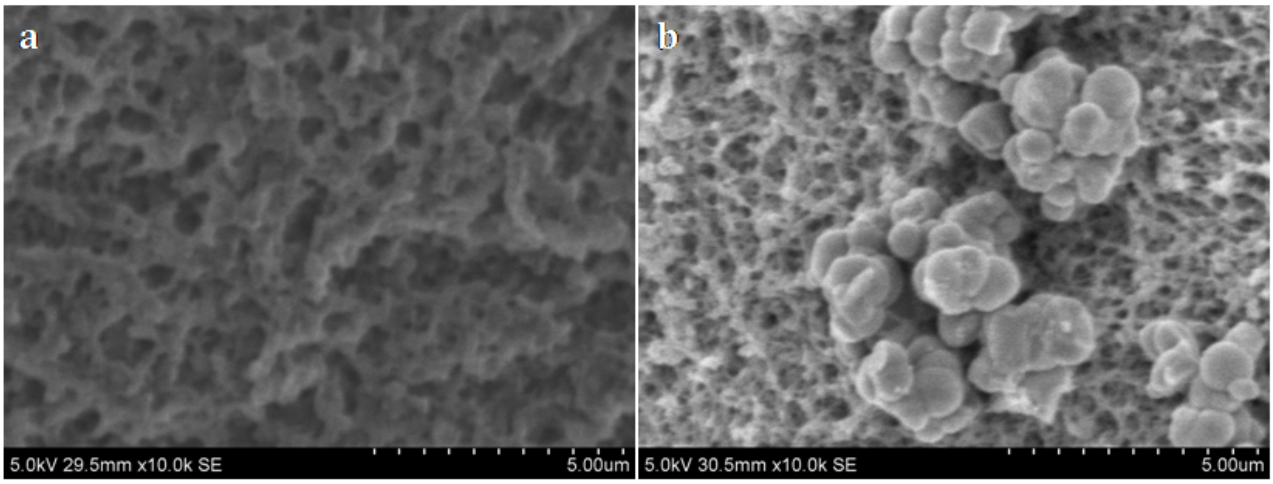

Figure 7

SEM analysis of (a) pure chitosan beads and (b) TA-0.5 coated chitosan beads, freeze-dried for 1 hour.

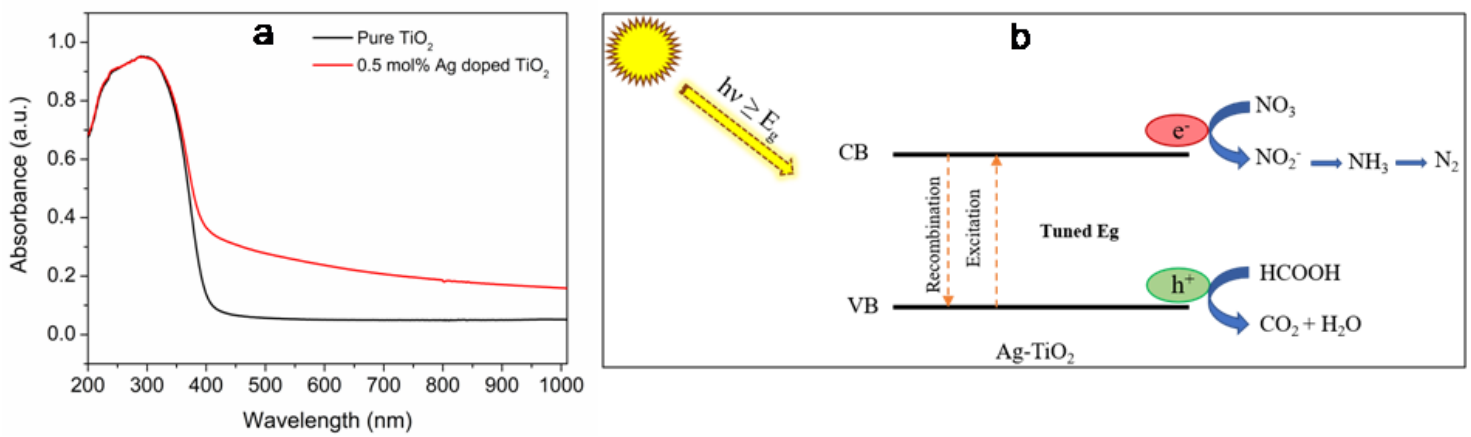

Figure 8

(a) UV-visible absorbance spectra of pure TiO2, Ag doped TiO2 and (b) Mechanism behind the photocatalytic nitrate reduction reaction using Ag modified titanium dioxide.

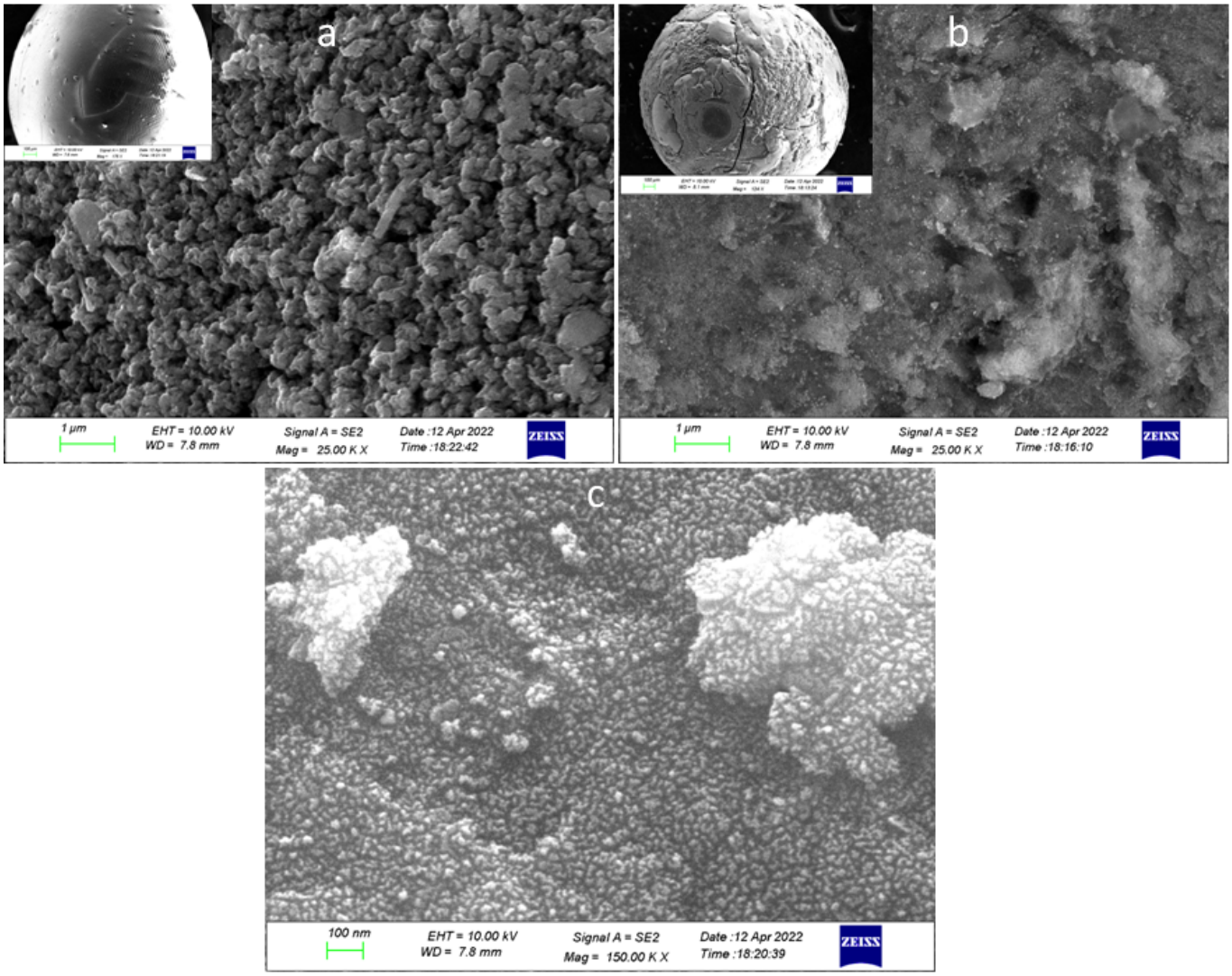

Figure 9

SEM morphology of (a) pure chitosan beads (b) Ag doped TiO2coated chitosan beads (CTA-0.5) and (c) high resolution image of ‘b’, both dried under oven conditions.

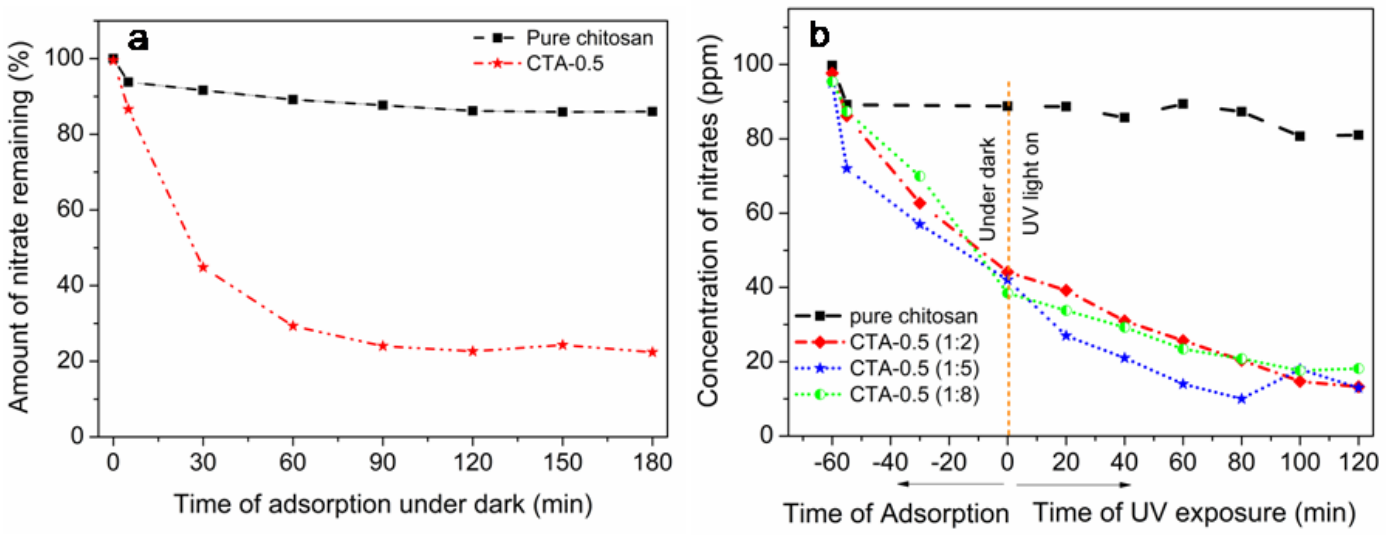

Figure 10

(a) Adsorption of nitrate ions under dark conditions by pure chitosan beads and Ag-doped TiO2 coated chitosan beads and (b) adsorption cum UV-photocatalysis by pure chitosan beads and Ag-doped TiO2 coated chitosan beads (both oven-dried) with nitrate: formate ratio 1:0 and 1:5

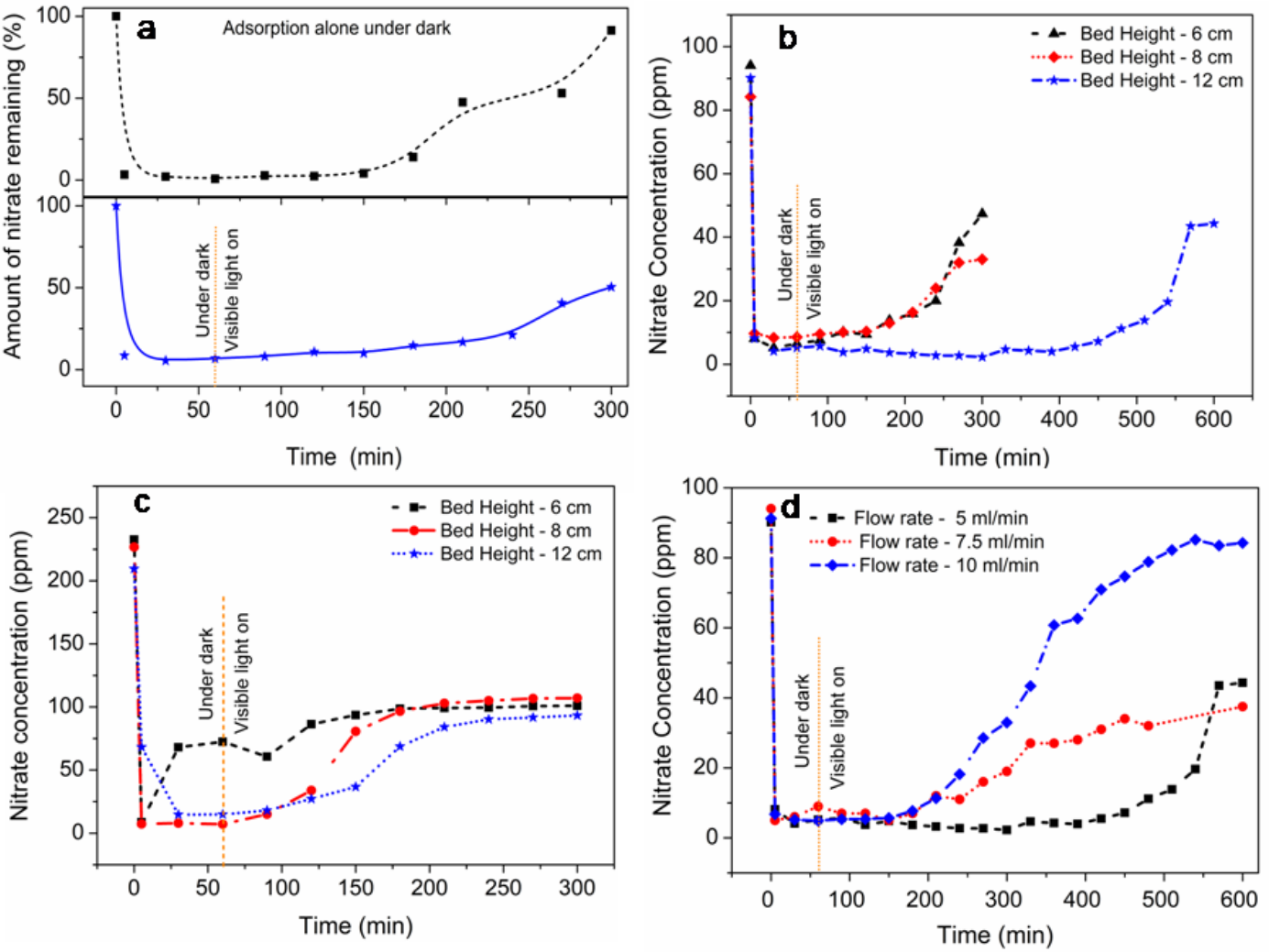

Figure 11

Fixed bed continuous flow adsorption cum photocatalytic studies using the oven dried CTA-0.5 nanocomposite beads (a) comparison between adsorption vs adsorption cum photocatalysis for a bed height 6cm, initial concentration-100 ppm and 5 ml min-1flow rate (b, c) effect of bed height and effect of initial concentration on the adsorption cum photocatalysis at a constant flow rate of 5 ml min-1and (d) effect of flow rate on the adsorption cum photocatalysis for a bed height 12 cm and initial concentration 100 ppm.

Supplementary Files

This is a list of supplementary files associated with this preprint. Click to download.

- Highlights.docx
- SupplememtaryInformation.docx